LETTERS
PUBLISHED ONLINE: 31 AUGUST 2014 | DOI: 10.1038/NNANO.2014.177
nature nanotechnology

Large negative differential conductance in single-molecule break junctions

Mickael L. Perrin[1], Riccardo Frisenda[1], Max Koole[1], Johannes S. Seldenthuis[1], Jose A. Celis Gil[1], Hennie Valkenier[2,3], Jan C. Hummelen[2], Nicolas Renaud[4], Ferdinand C. Grozema[4], Joseph M. Thijssen[1], Diana Dulić[1,5] and Herre S. J. van der Zant[1]*

Molecular electronics aims at exploiting the internal structure and electronic orbitals of molecules to construct functional building blocks[1]. To date, however, the overwhelming majority of experimentally realized single-molecule junctions can be described as single quantum dots, where transport is mainly determined by the alignment of the molecular orbital levels with respect to the Fermi energies of the electrodes[2] and the electronic coupling with those electrodes[3,4]. Particularly appealing exceptions include molecules in which two moieties are twisted with respect to each other[5,6] and molecules in which quantum interference effects are possible[7,8]. Here, we report the experimental observation of pronounced negative differential conductance in the current–voltage characteristics of a single molecule in break junctions. The molecule of interest consists of two conjugated arms, connected by a non-conjugated segment, resulting in two coupled sites. A voltage applied across the molecule pulls the energy of the sites apart, suppressing resonant transport through the molecule and causing the current to decrease. A generic theoretical model based on a two-site molecular orbital structure captures the experimental findings well, as confirmed by density functional theory with non-equilibrium Green's functions calculations that include the effect of the bias. Our results point towards a conductance mechanism mediated by the intrinsic molecular orbitals alignment of the molecule.

Negative differential conductance (NDC), characterized by a decrease in current with increasing voltage, is a widely used feature in electronic semiconductor devices. NDC has also been observed in molecular devices based on self-assembled monolayers (SAMs) and on single molecules[9–13]. In some devices the NDC effect could be explained by features of the electrodes or the interface[9,10], or by bias-dependent barriers[12], while in others it has been attributed to intramolecular features such as spin or phonon blockade[11], or conformational switching[13]. In most cases the NDC effects have been rather small, and large NDC effects (with a peak-to-valley ratio exceeding 2) have only been observed in SAMs[14,15], where they are due to chemical[16] or redox[17] reactions inside the SAM or traps at the electrode interface[18].

We investigate an intrinsic and pronounced NDC effect in a single thiolated arylethynylene molecule with a 9,10-dihydroanthracene core (AH, Fig. 1a)[19]. The molecule is studied using mechanically controllable break junctions (MCBJs), which offer high electrode stability and fine-tuning of the electrode spacing[20]. This control is realized by bending a flexible substrate in a three-point bending geometry (Fig. 1c). On bending the substrate, the gold wire deposited on top (see scanning electron microscopy (SEM) image in Fig. 1d) is stretched until it breaks. The two sides of the broken wire then act as electrodes, the separation of which can be adjusted with picometre resolution[21]. The molecules were deposited on the unbroken gold electrodes using self-assembly from a 0.1 mM solution in dichloromethane for 24 h. The set-up was pumped to a pressure below 5×10^{-6} mbar and cooled to a temperature of 6 K, after which current–voltage (I–V) characteristics were recorded. For comparison, we also performed detailed studies on a molecule with an anthracene core, which, in contrast to AH, is fully conjugated[19] (AC, Fig. 1b). For more details about the experimental procedures, see Supplementary Section IA.

Figure 2a presents a typical I–V curve measured in a device exposed to a solution of AH (sample A). At low bias, the current exhibits a pronounced NDC feature: starting from zero bias, the current initially increases, but, after 60 mV, it sharply decreases. The I–V characteristic is nearly symmetric around zero bias, with a similar peak occurring at −60 mV. At higher bias (Fig. 2b), the current increases again, and the I–V curve has the characteristic shape corresponding to tunnelling through a single barrier. The thin black line in Fig. 2b is a fit of the experimental I–V characteristic to the Simmons model[22].

We have also recorded I–V characteristics at various electrode spacings[23]. Figure 2c,d shows the results for sample A. These figures show that the NDC feature is tunable by mechanical control of the electrode distance. This mechanical tuning can be seen most clearly in the I–V characteristics of Fig. 2c. The NDC feature is very pronounced at short electrode separation (d_0) and remains visible when the electrode separation increases by more than 1 Å. The maximum current decreases with increasing electrode separation, for both positive and negative bias voltage. The tunnelling background follows a similar trend. The inset in Fig. 2b shows the background current as measured at 1 V as a function of electrode separation. The linear dependence in this semi-logarithmic plot confirms that the background can be described by a single tunnelling barrier where the width increases when increasing the electrode spacing. The peak-to-valley ratio increases from 3.0 to 7.1 with increasing electrode spacing, while the peak position shifts slightly outward. Figure 2d presents a current map in which the electrode spacing is successively increased and decreased. The total measurement took almost 9 h, and did not show any significant changes, demonstrating the stability of the NDC effect. Supplementary Section I.B presents data recorded in a similar way on two other samples.

In the abovementioned experiments, the electrodes were displaced over about one-tenth of a nanometre without fusing the

[1]Kavli Institute of Nanoscience, Delft University of Technology, Lorentzweg 1, 2628 CJ Delft, The Netherlands, [2]Stratingh Institute for Chemistry and Zernike Institute for Advanced Materials, University of Groningen, Nijenborgh 4, 9747 AG Groningen, The Netherlands, [3]School of Chemistry, University of Bristol, Cantocks Close, Bristol BS8 1TS, UK, [4]Department of Chemical Engineering, Delft University of Technology, Julianalaan 136, 2628 BL Delft, The Netherlands, [5]Departamento de Física, Facultad de Ciencias Físicas y Matemáticas, Universidad de Chile, Santiago de Chile, Chile. *e-mail: h.s.j.vanderzant@tudelft.nl

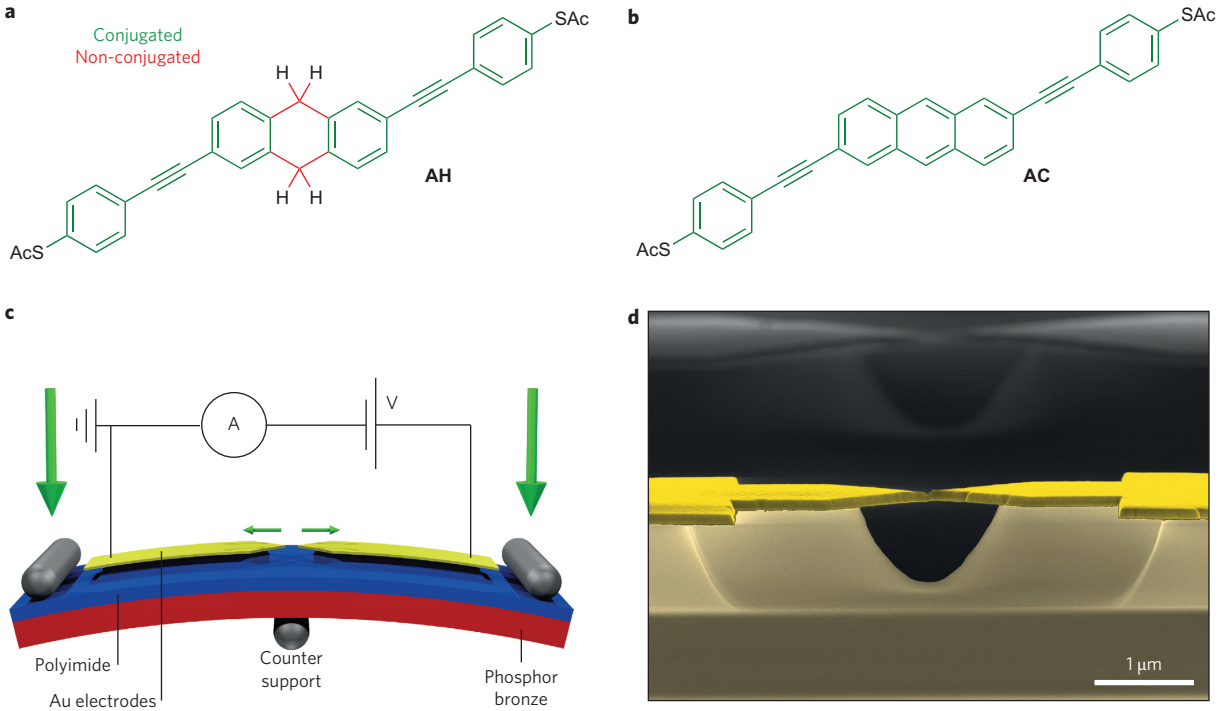

Figure 1 | Illustration of the experiment. a, Structure of a thiolated arylethynylene with a 9,10-dihydroanthracene (AH) core. To emphasize the broken conjugation of the molecule, the conjugated parts are shown in green, and the non-conjugated parts in red. **b**, Structure of a thiolated arylethynylene with an anthracene core (AC). Green bonds indicate that the molecule is fully conjugated. **c**, Layout of the MCBJ set-up. Large vertical green arrows represent the force applied to bend the sample. Small green arrows illustrate the attenuated electrode displacement as a result of bending. Current through the molecular junction is recorded upon application of a bias voltage. **d**, Colourized SEM image of an MCBJ device.

electrodes to study the stability of the junction. To investigate to what extent the molecular configuration is important for the observation of NDC, we repeatedly broke and fused the electrodes to create a new molecular junction in each cycle. While breaking, we recorded I–V characteristics for increasing electrode spacing[24]. This approach thus combines the advantages of spectroscopy of the molecular levels with a statistical assessment of the variation in the molecular junction formation. In the following, we will refer to this method as the 'I–V breaking series', that is, the series of measurements for which the electrodes are fused before each breaking event. This is to be contrasted to the I–V series described in the previous paragraphs and presented in Fig. 2, in which the electrodes are not fused.

Figure 3a presents I–V characteristics measured during a particular breaking event for increasing inter-electrode spacing. As in Fig. 2c, the NDC effect is clearly visible and it persists up to the largest electrode separation, while the low-bias conductance changes over several orders of magnitude. By linearly fitting the current at low bias, a conductance breaking trace can be constructed, as shown in Fig. 3b. In this plot the electrode displacement is set to zero at the rupture point of the last metallic atomic contact, for which the conductance quantization shows up as a plateau at G_0. With increasing electrode separation, the mono-atomic gold chain breaks, leading to a drop in conductance and the formation of a molecular junction. Upon further breaking, the conductance gradually decreases.

To perform a statistical analysis of the occurrence of NDC, we measured I–V series during 693 breaking events in total, recorded in three different samples (see Supplementary Section I.C for more details). We distinguish three types of series: (1) series without a molecule (tunnelling I–V characteristics with no plateau in the conductance trace); (2) series with a molecule but without NDC (I–V characteristics that show steps, or I–V characteristics with a plateau in the conductance versus displacement trace) and (3) series with a molecule and NDC. In 503 cases (72.6% of the events) no molecule was trapped between the electrodes, but 190 traces (27.4% of all the series) show molecular features. Of these 190 traces, 144 (~75% of the molecular junctions) exhibited NDC, with peak-to-valley ratios ranging from 1.5 to 15.

Using the same I–V breaking series approach, we performed measurements on the conjugated AC molecule (Fig. 3c,d). Figure 3c shows typical I–V characteristics for increasing inter-electrode spacing. The characteristics are monotonic and do not show NDC. Looking at the breaking trace shown in Fig. 3d, a plateau at G_0 is again visible, followed by a drop in conductance. A plateau in the conductance trace is then visible, indicating that a molecular junction has been formed (blue dots). For increasing displacement a conductance plateau is observed, after which the conductance drops sharply (red dots). We find that in ~33% of the breaking traces (510 series in total; three different samples), molecules are present in the junction. In those 170 junctions, 166 show no NDC. In the remaining four, NDC is observed.

In summary, a comparison of the measurements conducted on the two molecules reveals two distinct differences. First, the evolution of the conductance for increasing electrode distance is gradual for AH, spanning a wide range of conductances, whereas for AC a clear step is observed. Second, the statistics show that the NDC effect is very prominent in AH (75% where a molecular junction is formed) and almost absent in AC (2%).

To gain more insight into the origin of the NDC effect, we also investigated AH using density functional theory (DFT) and the non-equilibrium Green's function formalism (NEGF). Calculations were performed for the molecule in the gas phase using the Amsterdam density functional (ADF) quantum chemistry package with the GGA exchange-correlation functional and the

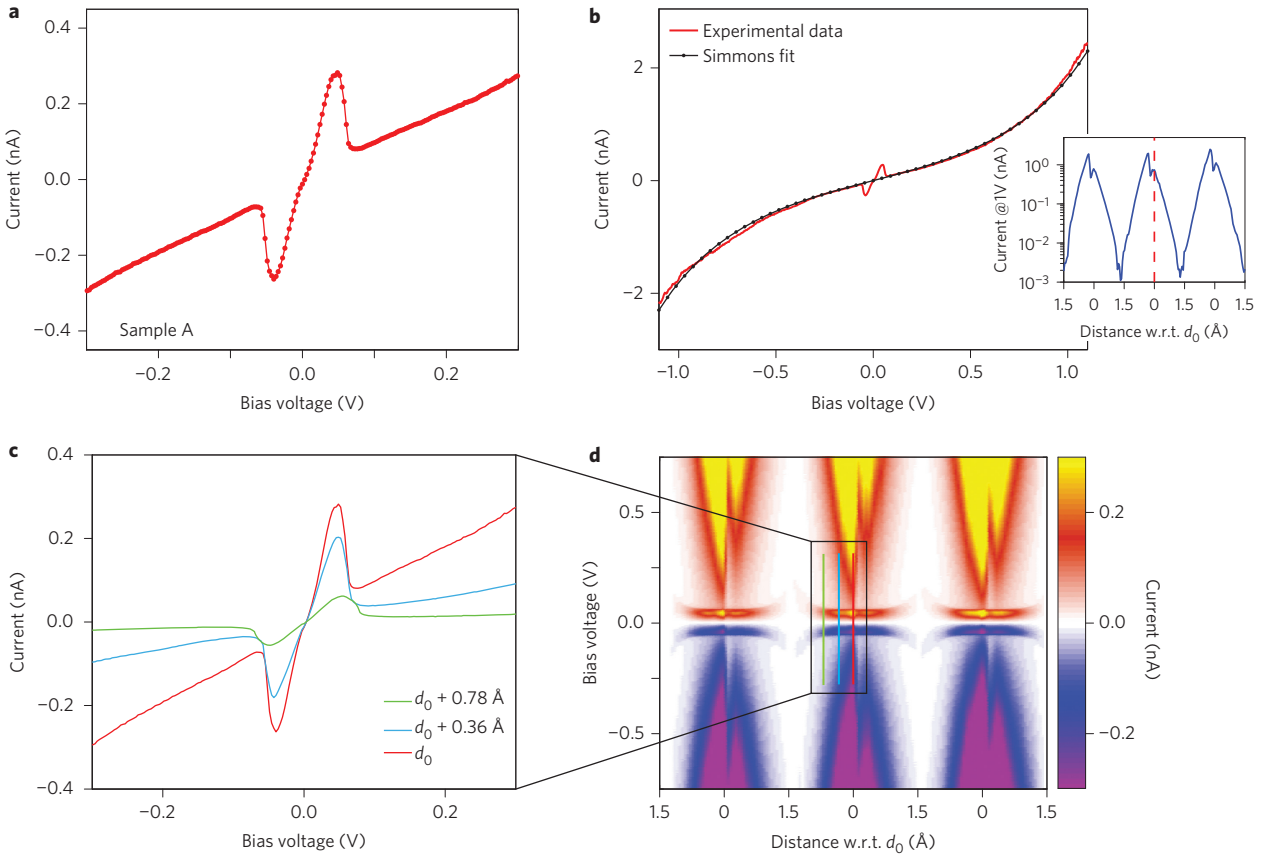

Figure 2 | NDC effect: mechanical tunability and stability. a,**b**, Typical *I*–*V* characteristic for low bias (**a**) and the full bias range (**b**). The black line is a fit to the Simmons model, with an electrode spacing of 11.0 Å. **c**, Low-bias *I*–*V* characteristics for increasing electrode separation. **d**, Map of *I*–*V* characteristics recorded from left to right while repeatedly increasing and reducing the electrode spacing. The spacing is relative to d_0, the electrode separation at which the NDC feature is most pronounced. The *I*–*V* traces shown in **c** are recorded at the positions marked by the coloured lines in **d**.

triple-ξ plus polarization basis set[25,26]. For details concerning the DFT calculation and the estimation of the parameters, see Supplementary Section II.B. Previous studies show that, for this molecule, transport is dominated by the highest occupied molecular orbital (HOMO) as it is closest to the Fermi energy (ϵ_F)[27]; the lowest unoccupied molecular orbital (LUMO), on the other hand, is located ~2.5 eV above ϵ_F. Inspection of the spectrum reveals that the HOMO and HOMO-1 are nearly degenerate (with an energy spacing $\Delta = 18$ meV) and that they have bonding/antibonding character[28]. This directly reflects the chemical composition of the AH molecule, which consists of two conjugated arms, connected by a non-conjugated segment (Fig. 1a). To see this, we transform the HOMO and HOMO-1 into an equivalent set of localized molecular orbitals (LMOs)[7] by addition and subtraction. This leads to one LMO located on the left half of the molecule and the other on the right half, as shown in Fig. 4a. The two LMOs can be viewed as two units in series, which are weakly coupled. Transport through the molecule can therefore be described using a model consisting of two sites, coupled to each other via a small coupling parameter τ (Fig. 4b). This intersite coupling can be estimated from the energy difference Δ between the HOMO and HOMO-1, which is obtained from DFT as $\tau = 9.1$ meV. The tunnel coupling of each site to its lead is characterized by Γ.

The NDC effect can be readily explained from such a two-site model[7,28–30]. At zero bias, the two sites are in resonance with each other and the conductance is high (Fig. 4b). Upon application of a bias voltage V, however, the energies of the two sites shift in opposite energy directions due to the Stark effect (Fig. 4c). DFT calculations in the presence of an electric field across the molecule show that a fraction α of the bias drops inside the molecule. When the two LMOs shift apart and $\alpha eV \gg 2\tau$, the current is substantially suppressed and the NDC feature sets in. For this two-site model, the current through the two-sites system can be calculated analytically using NEGF (see Supplementary Section II.A, where we also show that the analytical *I*–*V* is reproduced by DFT + NEGF calculations). In Fig. 4d we show an experimental *I*–*V* characteristic from which the background current has been subtracted and one calculated using the analytical expression of the two-site model. The excellent agreement supports the use of this model to describe transport through AH. Note that similar *ab initio* calculations on AC do not show an NDC effect, as expected from its conjugation, which extends across the whole molecule.

The calculation in Fig. 4d takes the two sites to be in resonance with the Fermi energy at zero bias and assumes the voltage drop across the electrode–molecule tunnel barriers to be symmetric over the junction, as this matches the observed *I*–*V* characteristics of more than half of the *I*–*V* breaking series. In the remaining measurements (see Supplementary Section II.D for more details and the statistics) the *I*–*V* characteristics show a gap at low bias. The presence of a gap can be explained by the sites being slightly off-resonant with the Fermi energy at zero bias. Our experiments therefore allow for quantification of the level alignment in a statistical way. If we assume a symmetric division of the applied voltages across the contacts, we find that the misalignment ranges from 0 to 225 meV. We further note that the NDC feature is also reproduced when considering more detailed quantum chemistry calculations involving the full self-energies of the metal electrodes

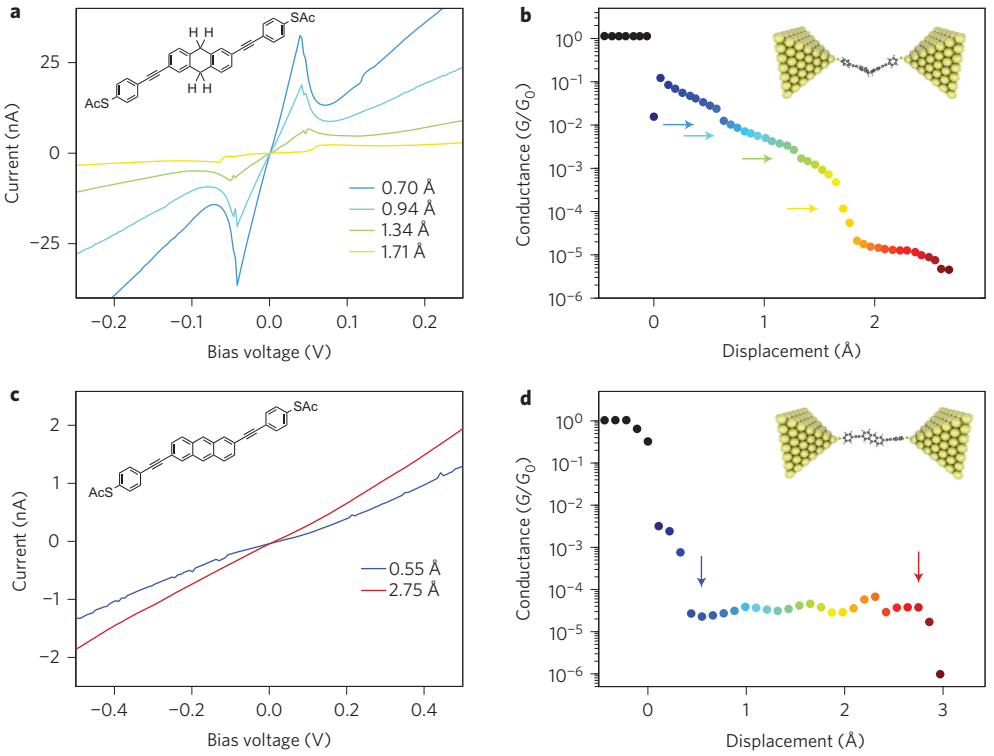

Figure 3 | *I–V* breaking series on AH and AC. a,**c**, *I–V* characteristics recorded during one breaking event on AH (**a**) and AC (**c**). **b**,**d**, Breaking traces showing the low-bias conductance versus electrode displacement obtained by a fit on each *I–V* characteristic in an *I–V* breaking series recorded on a junction exposed to AH (**b**) and AC (**d**). Coloured arrows indicate the location in the breaking trace at which the *I–V* characteristics in **a** and **c**, respectively, are recorded. Insets: possible junction configurations, as obtained from molecular dynamics simulations.

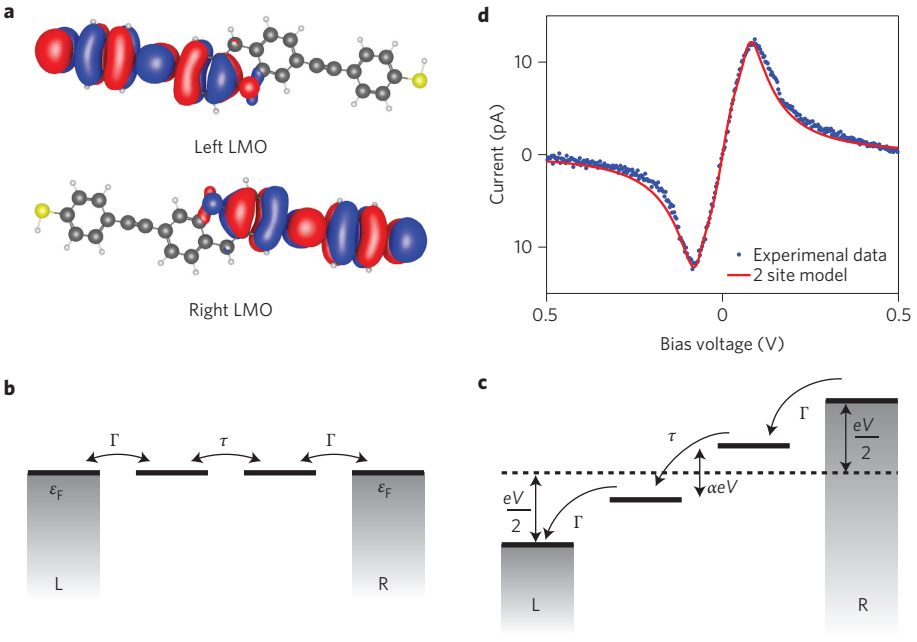

Figure 4 | Two-site model. a, The left and right LMO obtained by taking the sum and the difference of the HOMO and HOMO-1 (Supplementary Fig. 4). **b**, The LMOs are each located on one side of the molecule, so the junction can be modelled by two sites in series, left and right, coupled by τ. The sites are coupled to the leads by Γ. In the strong-coupling regime, transport through the molecule is coherent. Due to the symmetry of the molecule, the two sites, at ϵ_L and ϵ_R, are in resonance at zero bias and the conductance is high. **c**, Upon application of a bias, the sites are pulled off resonance by αeV, where α is the fraction of the voltage drop occurring inside the molecule. Although τ does not change significantly as a function of bias voltage, the off-resonance condition leads to a reduction of elastic transport through the molecule, lowering the conductance of the junction. **d**, Background-corrected *I–V* characteristics recorded on sample A with a fit to the two-site model using $\alpha = 0.74$, $\tau = 24.1$ meV and $\Gamma = 10.2$ meV. To match the absolute values of current, a prefactor of 7.2×10^{-5} was used.

and with a potential difference applied on the gold electrodes using the BAND package[31] (Supplementary Section II.C).

An intriguing aspect of the experiment is the gradual decrease of the conductance with increasing electrode separation, without the presence of clear conductance plateaux. Conductance histograms for AH at room temperature do indicate conductance plateaux below 1×10^{-6} G_0 (refs 24,28), which are not accessible in our experiments. It is important to realize that there is a distinct difference between the AH and AC molecules. AC is a rigid molecule, whereas AH can bend in the middle because of the broken conjugation. Molecular dynamics (Supplementary Section III) simulations confirm this and show that the junction evolves differently for the two molecules during breaking. AC, being rigid, remains in a planar configuration during the stretching of the electrodes, as illustrated in the inset of Fig. 3d. AH, on the other hand, shows a gradual evolution from a bent geometry (Fig. 3b) to a more planar configuration for larger separations. During this process, parameters τ, Γ and α, which determine the conductance, gradually change (Supplementary Section II.E). In particular the variation of τ may explain the gradual conductance decrease.

We finally note that AH is a symmetric molecule, so the two sites are on resonance with each other at zero bias. Introducing an asymmetry into the molecule can shift the sites apart, significantly changing the behaviour of the device. For example, if at zero bias the left site is higher in energy than the right site, a negative bias voltage would only pull them further apart (compare with Fig. 4d). They would therefore never move into resonance and the current remains low. At positive bias, on the other hand, they would align at a particular bias, increasing the current dramatically until the bias is so large that they are pulled off resonance again and the current decreases. This difference in behaviour at positive and negative bias means that such a molecule acts as a rectifier. We note here that unlike most reports on single-molecule diodes[32,33], this rectification is also present in the case of symmetric couplings to the leads. DFT + NEGF calculations on a particular asymmetric AH derivative (Supplementary Section II.F) indeed confirm this rectifying concept, with rectification ratios on the order of 400. Our findings thus show that the intrinsic molecular structure can introduce more complex molecular functionality, which may also contain multiple weakly coupled sites.

Received 24 September 2013; accepted 21 July 2014; published online 31 August 2014

References

1. Aviram, A. & Ratner, M. A. Molecular rectifiers. *Chem. Phys. Lett.* **29,** 277–283 (1974).
2. Moth-Poulsen, K. & Bjornholm, T. Molecular electronics with single molecules in solid-state devices. *Nature Nanotech.* **4,** 551–556 (2009).
3. Quek, S. Y. *et al.* Mechanically controlled binary conductance switching of a single-molecule junction. *Nature Nanotech.* **4,** 230–234 (2009).
4. Diez-Perez, I. *et al.* Controlling single-molecule conductance through lateral coupling of π-orbitals. *Nature Nanotech.* **6,** 226–231 (2011).
5. Venkataraman, L., Klare, J. E., Nuckolls, C., Hybertsen, M. S. & Steigerwald, M. L. Dependence of single-molecule junction conductance on molecular conformation. *Nature* **442,** 904–907 (2006).
6. Mishchenko, A. *et al.* Influence of conformation on conductance of biphenyl-dithiol single-molecule contacts. *Nano Lett.* **10,** 156–163 (2010).
7. Guedon, C. M. *et al.* Observation of quantum interference in molecular charge transport. *Nature Nanotech.* **7,** 304–308 (2012).
8. Vazquez, H. *et al.* Probing the conductance superposition law in single-molecule circuits with parallel paths. *Nature Nanotech.* **7,** 663–667 (2012).
9. Xue, Y. *et al.* Negative differential resistance in the scanning-tunneling spectroscopy of organic molecules. *Phys. Rev. B* **59,** R7852–R7855 (1999).
10. Guisinger, N. P., Greene, M. E., Basu, R., Baluch, A. S. & Hersam, M. C. Room temperature negative differential resistance through individual organic molecules on silicon surfaces. *Nano Lett.* **4,** 55–59 (2004).
11. Heersche, H. B. *et al.* Electron transport through single Mn_{12} molecular magnets. *Phys. Rev. Lett.* **96,** 206801 (2006).
12. Tu, X., Mikaelian, G. & Ho, W. Controlling single-molecule negative differential resistance in a double-barrier tunnel junction. *Phys. Rev. Lett.* **100,** 126807 (2008).
13. Gaudioso, J., Lauhon, L. J. & Ho, W. Vibrationally mediated negative differential resistance in a single molecule. *Phys. Rev. Lett.* **85,** 1918–1921 (2000).
14. Kratochvilova, I. *et al.* Room temperature negative differential resistance in molecular nanowires. *J. Mater. Chem.* **12,** 2927–2930 (2002).
15. Mentovich, E. D. *et al.* Multipeak negative-differential-resistance molecular device. *Small* **4,** 55–58 (2008).
16. He, J. & Lindsay, S. On the mechanism of negative differential resistance in ferrocenylundecanethiol self-assembled monolayers. *J. Am. Chem. Soc.* **127,** 11932–11933 (2005).
17. Chen, J., Reed, M. A., Rawlett, A. M. & Tour, J. M. Large on–off ratios and negative differential resistance in a molecular electronic device. *Science* **286,** 1550–1552 (1999).
18. Chen, J. *et al.* Negative differential resistance effect in organic devices based on an anthracene derivative. *Appl. Phys. Lett.* **89,** 083514 (2006).
19. Fracasso, D., Valkenier, H., Hummelen, J. C., Solomon, G. C. & Chiechi, R. C. Evidence for quantum interference in SAMs of arylethynylene thiolates in tunneling junctions with eutectic Ga-In (eGaIn) top-contacts. *J. Am. Chem. Soc.* **133,** 9556–9563 (2011).
20. Van Ruitenbeek, J. M. *et al.* Adjustable nanofabricated atomic size contacts. *Rev. Sci. Instrum.* **67,** 108–111 (1996).
21. Kergueris, C. *et al.* Electron transport through a metal–molecule–metal junction. *Phys. Rev. B* **59,** 12505–12513 (1999).
22. Simmons, J. G. Generalized formula for electric tunnel effect between similar electrodes separated by a thin insulting film. *J. Appl. Phys.* **34,** 1793 (1963).
23. Perrin, M. L. *et al.* Large tunable image-charge effects in single-molecule junctions. *Nature Nanotech.* **8,** 282–287 (2013).
24. Hong, W. *et al.* An MCBJ case study: the influence of π-conjugation on the single-molecule conductance at a solid/liquid interface. *Beilstein J. Nanotechnol.* **2,** 699–713 (2011).
25. Te Velde, G. *et al.* Chemistry with ADF. *J. Comput. Chem.* **22,** 931–967 (2001).
26. Fonseca Guerra, C., Snijders, J. G., te Velde, G. & Baerends, E. J. Towards an order-*N* DFT method. *Theor. Chem. Acc.* **99,** 391–403 (1998).
27. Kaliginedi, V. *et al.* Correlations between molecular structure and single-junction conductance: a case study with oligo(phenylene-ethynylene)-type wires. *J. Am. Chem. Soc.* **134,** 5262–5275 (2012).
28. Valkenier, H. *et al.* Cross-conjugation and quantum interference: a general correlation? *Phys. Chem. Chem. Phys.* **16,** 653–662 (2013).
29. Cornil, J., Karzazi, Y. & Bredas, J. Negative differential resistance in phenylene ethynylene oligomers. *J. Am. Chem. Soc.* **124,** 3516–3517 (2002).
30. Liu, R., Ke, S-H., Baranger, H. U. & Yang, W. Negative differential resistance and hysteresis through an organometallic molecule from molecular-level crossing. *J. Am. Chem. Soc.* **128,** 6274 (2006).
31. Verzijl, C. J. O. & Thijssen, J. M. DFT-based molecular transport implementation in ADF/BAND. *J. Chem. Phys. C* **116,** 24393–24412 (2012).
32. Loertscher, E. *et al.* Transport properties of a single-molecule diode. *ACS Nano* **6,** 4931–4939 (2012).
33. Batra, A. *et al.* Tuning rectification in single-molecular diodes. *Nano Lett.* **13,** 6233–6237 (2013).

Acknowledgements

This research was carried out with financial support from the Dutch Foundation for Fundamental Research on Matter (FOM), NWO/OCW, FP7-framework programme ELFOS, ERC grant no. 240299 and by an ERC advanced grant (Mols@Mols). The authors thank C. Verzijl for help with DFT calculations.

Author contributions

D.D. and H.v.d.Z. designed the project. M.P. fabricated the devices. H.V. and J.H. designed and provided the molecules. M.P. and M.K. performed the low-temperature *I–V* series without electrode fusion. M.P. and R.F. performed the low-temperature *I–V* breaking series. R.F. performed the room-temperature *I–V* breaking series. M.P., J.S., J.C.G. and J.T. performed the DFT + NEGF calculations. N.R. and F.G. performed the molecular dynamics simulations. M.P., J.S., J.T. and H.v.d.Z. wrote the manuscript. All authors contributed to the interpretation of the data and commented on the manuscript.

Additional information

Supplementary information is available in the online version of the paper. Reprints and permissions information is available online at www.nature.com/reprints. Correspondence and requests for materials should be addressed to H.S.J.v.d.Z.

Competing financial interests

The authors declare no competing financial interests.